NONDESTRUCTIVE TESTING AND EVALUATION, 2016
VOL. 31, NO. 3, 267–287
http://dx.doi.org/10.1080/10589759.2015.1111890

Taylor & Francis
Taylor & Francis Group

Pavement thickness and stabilised foundation layer assessment using ground-coupled GPR

Jinhui Hu[a], Pavana K. R. Vennapusa[a], David J. White[a] and Igor Beresnev[b]

[a]Department of Civil, Construction and Environmental Engineering, Iowa State University, Ames, IA, USA; [b]Department of Geological and Atmospheric Sciences, Iowa State University, Ames, IA, USA

ABSTRACT

Experimental results from field and laboratory investigations using a ground-coupled ground penetrating radar (GPR), dielectric measurement, magnetic imaging tomography (MIT) and dynamic cone penetrometer (DCP) tests are presented. Dielectric properties of asphalt pavement and stabilised and unstabilised pavement foundation materials were evaluated in the laboratory in frozen and unfrozen conditions. Laboratory test results showed that dielectric properties of materials back-calculated from GPR in comparison to dielectric gauge measurements are strongly correlated and repeatable. For chemically stabilised materials, curing time affected the dielectric properties of the materials. Field tests were conducted on asphalt pavement test sections with different foundation materials (stabilised and unstabilised layers), drainage conditions and layer thicknesses. GPR and MIT results were used to determine asphalt layer thicknesses and were compared with measured core thicknesses, while GPR and DCP were used to assess foundation layer profiles. Asphalt thicknesses estimated from GPR showed an average error of about 11% using the dielectric gauge values as input. The average error reduced to about 4% when calibrated with cores thicknesses. MIT results showed thicknesses that are about 9% higher than estimated using GPR. Foundation layer thicknesses could not be measured using GPR due to variations in moisture conditions between the test sections, which is partly attributed to variations in gradation and drainage characteristics of the subbase layer.

ARTICLE HISTORY
Received 24 June 2015
Accepted 12 October 2015

KEYWORDS
Ground penetrating radar; dielectric constant; asphalt pavement; layer thickness; moisture content

1. Introduction

Increasingly, non-destructive testing methods are being applied to assess pavement system conditions. According to the mechanistic empirical pavement design guide,[1] ground penetrating radar (GPR) surveys of existing pavements is a key assessment method for pavement rehabilitation design. Although primarily used for thickness determination, GPR scans are also used to identify defects (e.g. voids, stripping within the asphalt layer, weak bonds between pavement layers) within the pavement layers and beneath the pavement

CONTACT Pavana K. R. Vennapusa pavanv@iastate.edu

layer; determine depth and alignment of reinforcement in pavements; and determine air void content and density of asphalt layers.[2–11] Conducting GPR scans has the advantage of being rapid and less expensive compared to conducting test pits or borings to evaluate existing pavement conditions and it can provide continuous measurements along a pavement alignment. Validation of the GPR results, however, limits broader application of this technology, especially for pavement foundation layer assessment.

Dielectric properties of the pavement and foundation layer materials are key input parameters in determining layer thickness using GPR. The dielectric properties of layers are either assumed based on published typical values, determined from field calibrations[3] or measured directly using independent test devices.[12] Field calibration and direct measurement methods have proved successful for asphalt materials, although some studies have shown that variations in asphalt moisture content can affect the results.[3,4,12,13] For the underlying pavement foundation layer materials, however, the dielectric properties can vary significantly because of moisture and material property variations (e.g. clay content, moisture content, chemical stabiliser content, partially frozen/thawed, etc.). Previous research [13,14] has demonstrated that GPR data can be used to detect moisture variations within the foundation layers, but very limited data exist for stabilised foundation layers.

This study was undertaken with two objectives. The first objective was to evaluate the use of ground-coupled GPR to determine the asphalt and pavement foundation layer thicknesses, where an independent dielectric property measurement was used as an input. The second objective is to assess if ground-coupled GPR can be used to detect moisture variations and effects of freezing/thawing in the unstabilised and stabilised subbase, and subgrade layers beneath the pavement.

In situ tests were conducted on various asphalt pavement test sections with different foundation layer materials, drainage conditions and thicknesses.[15] The foundation layers included granular subbase layer underlain by stabilised (mechanically and chemically) or unstabilised subbase/subgrade layers. The pavement thicknesses *in situ* were measured from pavement cores and using a magnetic imaging tomography (MIT) gauge, and foundation layer thicknesses were measured using dynamic cone penetrometer (DCP). A laboratory experimental plan was designed to evaluate dielectric properties of chemically stabilised and unstabilised foundation materials in frozen and unfrozen conditions. To the authors' knowledge, this is the first paper to document dielectric properties of chemically stabilised materials and dielectric properties of pavement foundation layer materials in frozen and unfrozen conditions.

In the following sections of this paper, background information is presented on the basic principles of GPR and data analysis, field and laboratory data collection methods, followed by results and data analysis and then key findings from this study.

2. Background

2.1. Principles of GPR

GPR uses the principle of transmitting electromagnetic waves to locate changes in subsurface conditions. A detailed overview of GPR basic principles is provided by Daniels [16]. In brief, when an electromagnetic wave is transmitted from the antenna, it travels through the material at a velocity depending on the permittivity or dielectric constant of the material,

until it hits another object or material with different dielectric properties. When the wave hits a new object or a surface, part of the wave is 'reflected' back to the surface and is captured by the receiver, and part of the wave continues to travel downward until it is dissipated (or attenuated). The rate of signal attenuation depends on the dielectric properties and conductivity of the materials. If the materials are highly conductive (e.g. wet clays), the signal is attenuated rapidly.[17]

When a series of pulses are sent over a single point, then it is referred to as a scan. The strength or amplitude of the reflection is determined by the contrast in the dielectric constants of the two materials.[17] For example, when a pulse moves from dry sand (with a dielectric constant of about 5) to wet sand (with a dielectric constant of about 30), it will produce a strong reflection. On the other hand, when a pulse moves from dry sand to limestone (with a dielectric constant of about 7), it will not produce a strong reflection.

For pavement applications, 900 MHz to 2GHz antennas are typically used to provide information in the top 0.3–1 m. Most highway agencies use horn or air-coupled antennas where the antenna is located 150–500 mm above the surface. These antennas typically have a frequency range of 1–2 GHz. Ground-coupled antennas are in direct contact with the testing surface and typically have a maximum frequency of 1.5 GHz. The air-coupled antennas have advantage over ground-coupled antennas in obtaining data at highway driving speeds. However, as some of the electromagnetic waves sent by an air-coupled antenna are reflected back from the surface, the depth of penetration is generally lower than for a ground-coupled antenna with similar frequency.[2] Ground-coupled antennas limit the survey speed to walking speeds, however, to <10 km/h.

In ground-coupled antenna scans, the first positive peak produced in the data is referred to as 'direct coupling',[17] which occurs in the beginning of the scan and is used to identify the pavement surface position. The surface zero position is corrected in the data, by identifying this in the line scans.

2.2. Thickness determination using GPR

To determine thickness using GPR, the dielectric constant of the material is needed. The material dielectric constants can be estimated based on GPR signals or directly measured using hand-held test devices. There are two common ways to estimate dielectric constants of materials from GPR signals. One is to use the peak amplitude signals from each layer from a GPR scan in reference to the amplitude signal from a reflective metal surface, and the other is to use the two-way travel time in conjunction with known thickness values. The first method is applicable for air-coupled antennas,[6,13,18] which were not used in this study and are therefore not described here. The two-way travel time method, which is applicable for ground-coupled antennas, was used in this study. According to Loken [18], the two-way travel time method is not influenced by the errors associated with signal attenuations as with air-coupled methods.

The interval of time that it takes for the wave to travel from the transmitter to the receiver is called the two-way travel time. Using the two-way travel times between the different amplitude peaks observed in a wiggle scan, and known layer thickness values, the dielectric constant values can be determined using Equation (1) [19]:

$$\varepsilon = \left(\frac{ct_i}{2h_i}\right)^2 \tag{1}$$

where c = speed of light in air (0.30 m/ns), ε = dielectric constant or relative electrical permittivity, h_i = individual layer thickness and t_i = time travel in each individual layer.

Irrespective of the two test methods described above, a field calibration is first required wherein dielectric constant of the material is determined using direct thickness measurements. Using air-coupled GPR antennas, some previous studies [13,20–22] have documented average errors of about 6–10% when no core calibration was performed vs. 1–5% when core calibration was performed. Some researchers [20,23] have indicated that calibrating GPR data with at least three cores when compared to one core can substantially reduce the error.

As an alternative to field calibration, dielectric properties of the materials can be determined independent of GPR using hand-held test devices. However, there is no widely accepted method in terms of what test device should be used. Loizos and Plati [12] used a hand-held percometer device in determining dielectric properties of asphalt materials. They found that the location where the dielectric properties were measured (i.e. at the surface or in the middle or at multiple locations on a core) influenced the results. A dielectric probe manufactured by Adek, Ltd. was used by Saarenketo and Scullion [24]. In this study, a GS3 sensor manufactured by Decagon Devices, Inc. was used to measure dielectric properties of asphalt and foundation layer materials. Details of GS3 are provided later in this paper.

2.3. Moisture content determination in foundation layers

Moisture content influences the dielectric properties of the materials because the water dielectric constant is much higher (81) than that of air (1) or soil materials (4–20). Therefore, high dielectric constants of materials can be attributed to high moisture values [18].

Halabe et al. [25] used the complex refractive model (CRM) to evaluate relationships between dielectric properties of a material mixture, its volumetric ratios and dielectric properties of its components. Using the CRM, the gravimetric moisture contents of granular base materials can be obtained using Equation (2) [25]:

$$w = \left(\sqrt{\varepsilon_b} - 1 - \frac{1-n}{\sqrt{\varepsilon_s} - 1} \right) \Bigg/ \left(\sqrt{\varepsilon_b} - 1 - \frac{1-n}{\sqrt{\varepsilon_s} - 22.2} \right) \tag{2}$$

where w = moisture content determined as fractional weight of water to total weight; ε_s = dry aggregate dielectric constant; ε_b = base layer dielectric constant determined using the two-way travel time method (Equation (1)); and n = porosity = fractional volume of voids (air + water) to total volume.

To determine moisture contents from Equation (2), the porosity of the material has to be either measured or assumed. Maser and Scullion [26] used Equation (2) by measuring the dry unit weight of granular base material at one location for calibration and then used the same constant value to estimate moisture content at other locations. Comparison between the measured and the predicted moisture contents in their study resulted in root-mean-squared error of <2%.

Scullion et al. [27] reported a procedure that involved developing a laboratory relationship between gravimetric moisture content and dielectric constant to estimate moisture contents *in situ* from GPR scans. Results from their study indicated that the relationship

between dielectric content of the mixtures increased with increasing moisture content (as expected), and the relationships were unique for each material type.

Grote et al. [14] used field GPR scans to estimate the dielectric properties of the foundation layers from the two-way travel time method and then estimated material volumetric moisture contents based on laboratory relationships. Site- and material-specific relationships between volumetric moisture content and dielectric properties were used in their study for some materials. For materials where those relationships were not available, a third-order polynomial equation developed by Topp et al. [28] based on tests conducted over a wide range of material types (sandy loam to clay loam to organic soil to glass beads) as shown in Equation (3) was used:

$$\theta_v = 4.3 \times 10^{-6}\varepsilon^3 - 5.5 \times 10^{-4}\varepsilon^2 + 2.92 \times 10^{-2}\varepsilon - 0.053 \quad (3)$$

where θ_v = volumetric moisture content and ε = material dielectric constant.

3. Field test sections and experimental testing methods

3.1. Description of field test sections

The test site located in Boone, Iowa, was specifically constructed in 2012–2013 to incorporate several experimental pavement test sections. The foundation layer construction details are summarised in White et al. [15]. The test site consists of 12 roads labelled from 1st St. to 12th St. A summary of pavement cross section with design thicknesses of each layer in all sections is provided in Table 1. Material properties of all foundation layer materials are summarised in Table 2.

All streets expect 6th St. were surfaced with a nominal 152-mm-thick hot mix asphalt (HMA) or warm mix asphalt (WMA) layer underlain by a nominal 152-mm-thick crushed limestone subbase (CLS) layer. Sixth St. is surfaced with Portland cement (PC) concrete pavement and the results are not included in this paper. The HMA and WMA layers varied between the test sections with the type of aggregate used in the mixture (i.e. low or high absorption aggregate, LAA or HAA) as summarised in Table 2.

Geocells were used within the CLS layer on 3rd St., and geotextiles and geogrids were used at the CLS and subgrade layer interface on 3rd, 4th and 5th St. sections. Natural or compacted subgrade layers were directly beneath the CLS layer on 1st, 3rd, 4th, 5th, 8th and 10th streets. On 2nd, 7th, 9th, 11th and 12th St. sections, either a stabilised or unstabilised reclaimed subbase (RSB) or subgrade layer was used between the CLS and subgrade layers, as summarised in Table 2. Stabilisation of subbase and subgrade layers was performed using mechanical stabilisation (i.e. mixing RSB and existing subgrade), or by adding PC or self-cementing Class C fly ash (FA). On 11th St. N, a geocomposite drainage layer was installed directly beneath the asphalt layer.

An array of temperature sensors (thermistors) were installed in the pavement and the foundation layers down to a depth of about 1.4 m below surface for near-continuous monitoring of temperature variations.

3.2. Field and laboratory testing methods

3.2.1. Field and laboratory GPR surveys

A GPR manufactured by Geophysical Survey Systems, Inc. (GSSI) was used in this study. GPR surveys were conducted on field test sections in March (winter/frozen ground) and

Table 1. Summary of field tests sections.

Section	Surface layer	Base layer	Intermediate layer	Subgrade layer
1st St. N and S	152-mm HMA with LAA[a]	152-mm CLS	–	Compacted subgrade
2nd St. N and S	152-mm HMA with LAA[a]	152-mm CLS	304-mm mechanically stabilised subgrade	Natural subgrade
3rd St. N	152-mm HMA with LAA[a]	152-mm CLS reinforced with 100-mm geocells	Non-woven geotextile	Natural subgrade
3rd St. S	152-mm WMA with LAA[a]	152-mm CLS reinforced with 150-mm geocells	Non-woven geotextile	
4th St. N	152-mm WMA with LAA[a]	152-mm CLS	Non-woven geotextile	Natural subgrade
4th St. S			Woven geotextile	
5th St. N	152-mm WMA with LAA[a]	152-mm CLS	Triaxial geogrid	Natural subgrade
5th St. S			Biaxial geogrid	
7th St. N and S	51-mm HMA with HAAb + 102-mm HMA with LAAa	152-mm CLS	152-mm 5% PC-stabilised reclaimed subbase	Natural subgrade
8th St.	51-mm HMA with HAA[b] + 102-mm HMA with LAAa	152-mm CLS	–	Compacted subgrade
9th St.	51-mm HMA with HAA[b] + 102-mm HMA with LAA[a]	152-mm CLS	152-mm reclaimed subbase	Natural subgrade
10th St. N	51-mm WMA with	152-mm CLS	–	Compacted subgrade
10th St. S	HAA[b] + 102-mm HMA with LAA		–	Natural subgrade
11th St. N	51-mm WMA with HAA[b] + 102-mm	152-mm CLS	12-in. 11.4% PC-stabilised subgrade	Natural subgrade
11th St. S	WMA with LAA		12-in. 22.3% FA-stabilised subgrade	

[a]Low absorption aggregate.
[b]High absorption aggregate.

Table 2. Summary of material index properties.

Parameter	CLS	RSB	Concrete sand	Iowa Loess	Glacial till subgrade
Gravel content (%) (>4.75 mm)	65.2	37.2	2.2	0.0	5.3
Sand content (%) (4.75 – 75 μm)	58.1	48.4	96.2	2.9	39.7
Silt + clay content (%) (<75 μm)	7.1	14.4	1.6	103.7	55.0
D_{10} (mm)	0.3	0.02	0.28	–	0.12
D_{30} (mm)	3.6	0.45	0.57	0.013	0.01
D_{60} (mm)	10.1	4.0	1.2	0.028	–
Coefficient of uniformity, C_u	33.7	160	4.22	–	–
Coefficient of curvature, C_c	4.3	2.0	0.95	–	–
Liquid limit, LL (%)	NP	NP	NP	29	33
Plasticity index, PI (%)				23	15
AASHTO classification	A-1-a	A-1-a	A-1-b	A-4	A-6(5)
USCS group symbol	GP-GM	SM	SP	ML	CL

September (fall) of 2014. A ground-coupled 900-MHz antenna setup with SIR-20 data acquisition system was used (Figure 1). Based on the manufacturer recommendations, the following scan settings were used: (a) range = 15 ns; (b) frequency of scans = 64 Hz; and (c) number of samples per scan = 512.

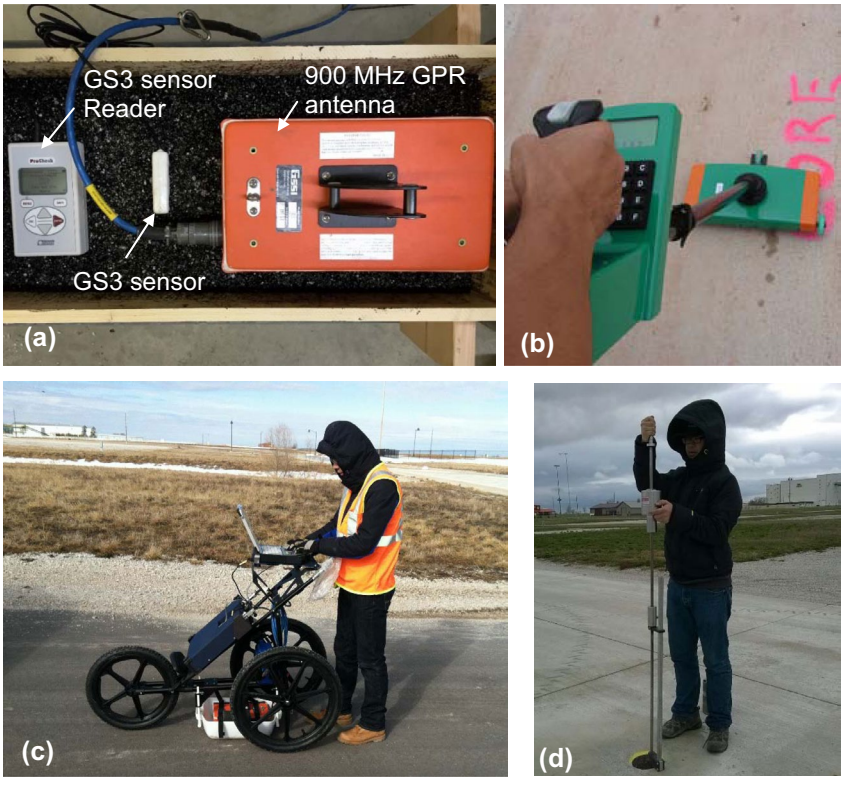

Figure 1. (a) Test setup using GS3 sensor and GPR antenna in laboratory box study; (b) MIT gauge; (c) GPR setup with a scanning survey wheel setup *in situ*; and (d) DCP testing of the foundation layer through a pavement core.

For *in situ* GPR scanning, a survey encoder was used to connect the GPR device with a calibrated survey wheel to measure the distance. For GPR scanning conducted in the laboratory box study (described in 3.2.6), scans were performed in point-mode setting (i.e. data are collected only over a single point).

3.2.2. Pavement coring

Iowa Department of Transportation (Iowa DOT) performed pavement coring at 58 locations in April 2014 in test sections shown in Table 1. The core thicknesses were measured in accordance with ASTM D3549. The core thicknesses are reported in this paper as h_{core}.

3.2.3. MIT gauge scanning

The working principle of the MIT gauge is described in detail in Grove et al. [29] and is manufactured by the MIT Measurement and Testing Technology (MIT Mess- und Prüftechnik) in Dresden, Germany. In brief, the MIT gauge generates a variant magnetic field that creates an eddy current in a metal reflector that is placed beneath the pavement. This eddy current will generate an induced magnetic field inside the metal reflector that can be detected by a sensor in the MIT gauge. Based on a calibration between the intensity of the induced magnetic field for a given type of reflector and the distance between the sensor and the

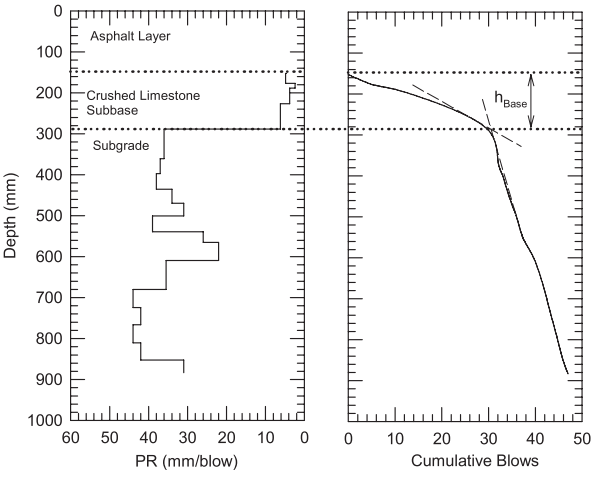

Figure 2. Example PR and cumulative blows with depth profiles used for base layer thickness determination.

metal reflector, the pavement thickness is calculated. The calibration is unique to the type of metal reflector used. Grove et al. [29] showed that the differences between the MIT gauge thickness measurements and core thickness measurements were 2 mm or less, based on 106 data points collected over 12 project sites.

A picture of the MIT gauge used in this study is shown in Figure 1. In this study, 0.6-mm-thick galvanised sheet metal circular discs supplied by the manufacturer were used. The metal discs were placed beneath the pavement at 109 selected locations that were marked with global positioning system (GPS).

3.2.4. Field DCP testing

DCP tests were conducted in the foundation layers shortly after the pavement cores were removed and at various test locations prior to paving (Figure 1). Tests were done at a total of 100 locations in accordance with ASTM D6951.[30] Penetration resistance (PR) and cumulative blows vs. depth plots were generated at each test point to determine the base layer thickness as illustrated in Figure 2. The base layer thickness was determined as depth from the bottom of the asphalt layer to the inflection point of the tangent of the lower portion of the cumulative blows with depth curve.

3.2.5. Dielectric constant determination

Dielectric constant of asphalt and foundation layer materials was directly measured using a GS3 sensor manufactured by Decagon Devices, Inc. (Figure 1) and was also estimated using the two-way travel time method as per Equation (1). The dielectric constant measured with the GS3 is reported as ε_{GS3}, while the dielectric constant estimated from Equation (1) is reported as ε_{GPR}.

The GS3 device uses capacitance/frequency domain technology to measure soil dielectric constant. The device uses an epoxy body and consists of three stainless steel needles, and has a thermistor to measure temperature. It uses an electromagnetic field to measure the dielectric permittivity of the surrounding medium.[31] The sensor supplies a 70-MHz oscillating wave to the sensor prongs that charge according to the dielectric properties of

the material. According to the manufacturer, the sensor has a measurement influence depth of about 10 cm.[31]

The GS3 sensor was used for the measurement of laboratory-compacted specimens and in field on the asphalt layers. The laboratory-compacted specimens for foundation materials were prepared by compacting materials in accordance with ASTM D698 [32] at various target moisture contents, to assess relationships between gravimetric moisture content (w) and ε_{GS3}. Laboratory testing was conducted on the following materials: loess, subgrade glacial till, CLS, RSB, and PC- and FA-treated glacial till subgrade. A nominal 10% PC and 20% FA (by dry weight of soil) was used for treatment, to match with field conditions. All compacted specimens, except the FA- and PC-treated subgrade samples, were tested immediately after compaction and after freezing for about 48 h at about −16°C. The PC- and FA-treated subgrade samples were tested at various times after compaction up to about 7 days to assess the influence of curing (i.e. time-dependent formation of cementitious reaction products that hold water) on ε_{GS3} measurements.

3.2.6. Laboratory box testing

Laboratory box testing was conducted in this study to evaluate the GS3 device by comparing ε_{GPR} and ε_{GS3} results for various materials compacted at different target moisture contents. A repeatability study on the two-way travel time method to estimate the ε_{GPR} was also conducted as part of the box study. The materials included Iowa loess, concrete sand, CLS and cold mix asphalt (CMA). The index properties of these materials are summarised in Table 2.

The materials were compacted in a 762 mm × 304.8 mm × 381 mm wooden box. A metal plate was placed at the bottom of the box as a reflection surface for GPR scans. Tests were conducted on uniform single layer of material with Iowa loess and concrete sand and two- and three-layered structures with loess, CLS and CMA. The layers were compacted in thin layers (<30-mm thick) using a hand tamper.

GPR scan and GS3 sensor measurements were simultaneously obtained on the different materials. The two- and three-layered structures were tested at room temperature and after freezing in a temperature chamber for 48 h (at about −18 °C) to assess the influence of frozen vs. unfrozen conditions.

3.3. Asphalt layer thickness determination In Situ

Asphalt layer thicknesses were determined from core measurements and using the MIT gauge. GPR scanning data were used to estimate the asphalt layer thicknesses at the core and MIT test locations for comparison with the measured thicknesses, using three procedures.

The first procedure involved the following steps: (1) measure ε_{GS3} from one location in each asphalt mixture type and assume the same at all core locations in the test sections with the same mixture type; (2) convert ε_{GS3} to ε_{GPR} using a relationship developed from the laboratory box study; (3) determine the two-way travel time from the GPR scan at each core location for the asphalt layer; and (4) use the two-way travel time and ε_{GPR} in Equation (1) to estimate the asphalt layer thickness (h_{GPR1}).

The second procedure involved the following steps: (1) determine two-way travel times at each core location in sections with same asphalt mixture type; (2) use Equation (1) and h_{core} at each location to calculate ε_{GPR}; (3) average those values for each asphalt mixture; (3) using the two-way travel time at each location and the average ε_{GPR}, estimate the asphalt

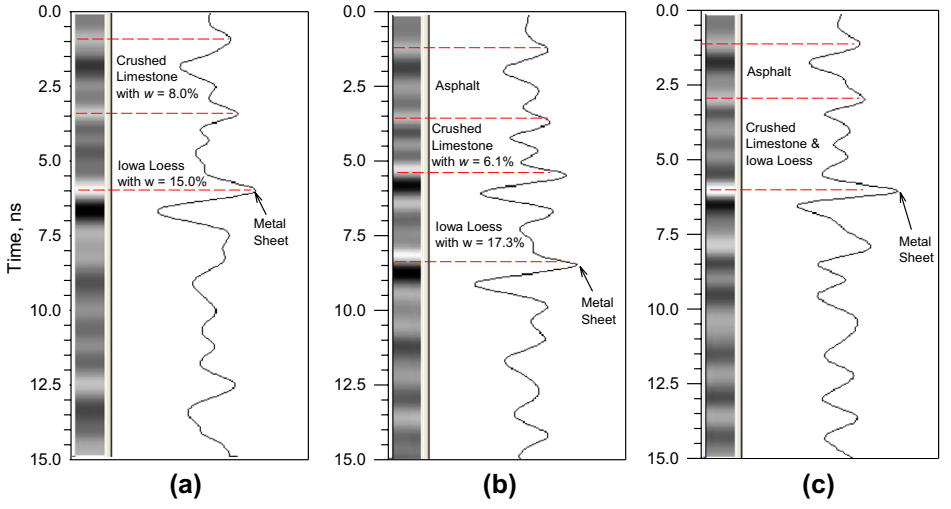

Figure 3. Results of laboratory box study with (a) two-layered profile at room temperature, (b) three-layered profile at room temperature and (c) three-layered profile frozen at −17.8 °C for 48 h.

layer thickness (h_{GPR2}). This procedure was used herein to assess the advantage of using average data (from multiple samples) over single point data as described below in the third procedure.

The third procedure involved the following steps: (1) determine two-way travel time from the GPR scan at one random core location for each asphalt mixture type; (2) use Equation (1) and the measured h_{core} at the location to determine ε_{GPR} and assume it is the same at all core locations in the test sections with the same mixture type; and (3) determine two-way travel time at the remaining core locations using Equation (1) to estimate the asphalt layer thickness (h_{GPR3}).

4. Results and discussion

4.1. Laboratory box study results

GPR scanning test results on two- and three-layered systems at room temperature and after freezing are presented in Figure 3. Moisture contents of the CLS and loess layers are noted in Figure 3. Comparison of results at room temperature and after freezing indicated different two-way travel times. For example, the two-way travel time to the metal sheet was about 8 ns at room temperature, while it was about 6 ns after freezing. In the frozen condition, the CLS/loess layer interface is not as well defined as when not frozen.

Results from the box study comparing ε_{GPR} and ε_{GS3} are shown in Figure 4, which yielded a linear regression relationship with coefficient of determination (R^2) = 0.95 and standard error (SE) = 1.3. As shown, the ε_{GS3} values are lower than ε_{GPR} values. The reasons for this difference are attributed to the differences in the measurement influence depths and the measurement errors associated with the two methods. ε_{GPR} represents an average value for the full depth of each layer, while ε_{GS3} only represents the surrounding medium in the depth of penetration.

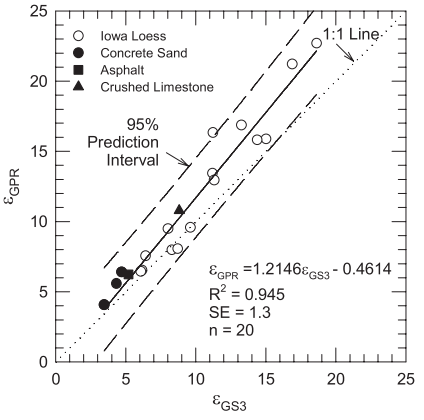

Figure 4. Comparison of dielectric constant values determined from GPR (E_{GPR}) and GS3 sensor (E_{GS3}).

Table 3. Summary of repeatability analysis test results in determining $\boldsymbol{\varepsilon}_{GPR}$ from two-way travel time.

	Two-layer system		Three-layer system in room temperature			Three-layer system in frozen condition	
Statistical parameters	CLS	Loess	CMA	CLS	Loess	CMA	CLS + Loess
Number of measurements	28	28	24	24	24	31	31
Average ε_{GPR}	11.02	12.74	6.55	6.12	15.57	4.87	4.73
Standard deviation or measurement error of ε_{GPR}	0.08	0.09	0.09	0.04	0.08	0.07	0.02
Coefficient of variation or percentage error*	0.7%	0.7%	1.4%	0.7%	0.5%	1.4%	0.4%

*calculated as 100 × standard deviation of ε_{GPR}/average ε_{GPR}.

The repeatability of the two-way travel time method to determine ε_{GPR} was evaluated by obtaining repeated measurements on two-layer and three-layer structures. The results are summarised in Table 3, which indicated that the measurement error of ε_{GPR} was <0.1 for all materials and the percentage error relative to the average value was <1.5%. The CLS and loess layers showed different dielectric constant values in two-layer and three-layer systems. The reason for this is attributed to differences in the material moisture contents.

4.2. Laboratory dielectric constant measurements on compacted specimens

Results showing ε_{GS3} vs. gravimetric moisture content (determined on batched materials) immediately after compaction and after freezing are shown in Figure 5. The results indicated that ε_{GS3} values increased with increasing gravimetric moisture content for all materials, as expected, and the relationship between ε_{GS3} and moisture content is unique for each material type. When frozen, the ε_{GS3} values ranged between 4 and 6 for all materials. This is expected because the dielectric constant in the ice phase of frozen water is about 3.2 [33].

Figure 6 shows ε_{GS3} vs. curing time for chemically stabilised specimens compacted at different moisture contents. ε_{GS3} increased with increasing moisture content and decreased with curing time up to about 12 h and then stayed relatively constant. The changes in ε_{GS3} with curing time is attributed to the hydration process where the amount of free water

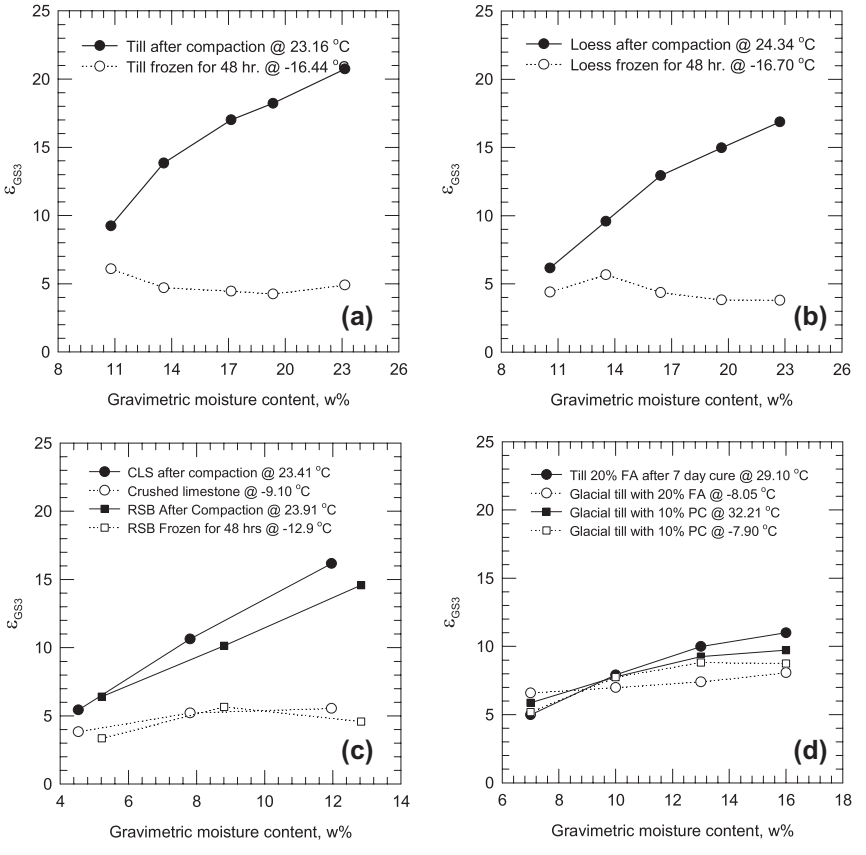

Figure 5. E_{GS3} vs. gravimetric moisture content on: (a) glacial till subgrade, (b) Iowa loess, (c) CLS and RSB and (d) glacial till treated with PC and FA.

decreases with curing. This was also observed by others that investigated the concrete hydration and curing process.[34]

The PC- and FA-stabilised subgrade produced lower dielectric constant values compared to unstabilised subgrade. For example, at about 16% gravimetric moisture content, the ε_{GS3} of the unstabilised subgrade was 16, while ε_{GS3} of the PC- and FA-stabilised subgrade was about 10.

4.3. Field test results

4.3.1. Asphalt layer

Results of GPR scans for a portion of a test section from the two testing times are shown in Figure 7. Ground temperatures are presented in Figure 8, which indicates the foundation layers were frozen in March up to a depth of about 1.3 m below the pavement surface. GPR scans obtained during March did not show a transition between subbase and subgrade layers. This confirmed the laboratory box study results.

The measured (h_{core}) and estimated (h_{GPR1}, h_{GPR2}, h_{GPR3}) asphalt layer thicknesses are compared in Figure 9. A comparison between the average measured and estimated thickness

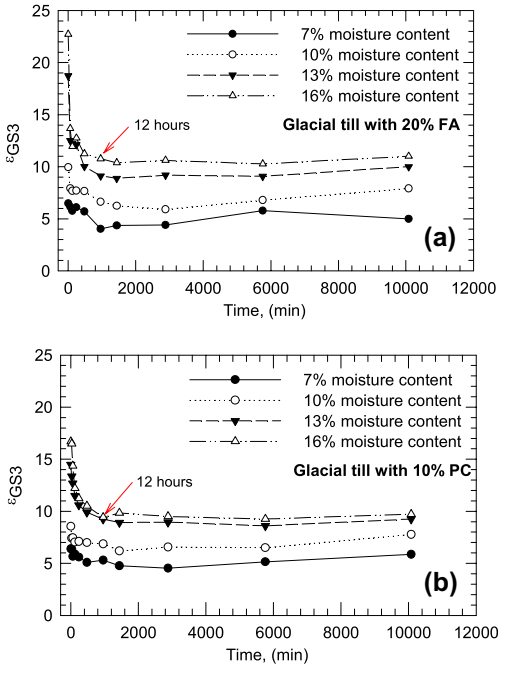

Figure 6. E_{GS3} on chemically stabilised till subgrade at different moisture contents after different curing times: (a) stabilised with 20% FA and (b) stabilised with 10% PC.

values for each asphalt mixture type and the average percentage error of the estimates relative to the average measured values is summarised in Table 4. The percentage error is calculated as the ratio of the root mean square error relative to h_{core} and the average h_{core}.

The h_{GPR1} values estimated using the ε_{GS3} values produced an average error of about 11%. The estimated h_{GPR2} and h_{GPR3} values produced values closer to the 1:1 line when compared with the measured values. The error values ranged between 2.7 and 8.6% for h_{GPR3}, depending on the core sample selected in the analysis. The average error reduced to about 3.7% for h_{GPR3}, when average ε_{GPR} was used for each material type. This suggests that if calibration is performed with more number of samples, the error in the predicted values can potentially be minimised. The percentage error values reported herein are similar to those reported by others with air-coupled antennas.[13,20–23]

Comparison between asphalt layer thickness measured using the MIT gauge and GPR (h_{GPR2}) is presented in Figure 10. h_{GPR2} was chosen here for comparison as the data were close to the 1:1 line when compared with h_{core} (Figure 9). Results indicated that MIT gauge thickness measurements were on average about 9% higher (i.e. about 15 mm) than estimated with GPR. The 15-mm error measured from testing on asphalt cores in this study is higher than reported in Grove et al. [29] study which was 2 mm from testing on concrete cores. A thorough future evaluation with a direct comparison between core thickness and MIT gauge is warranted.

4.3.2. Base/subbase layer

GPR scans from September 2014 identified the bottom of the granular base layer (CLS or CLS + RSB layer). On 9th St. test sections where CLS and RSB constitute the subbase layers, a

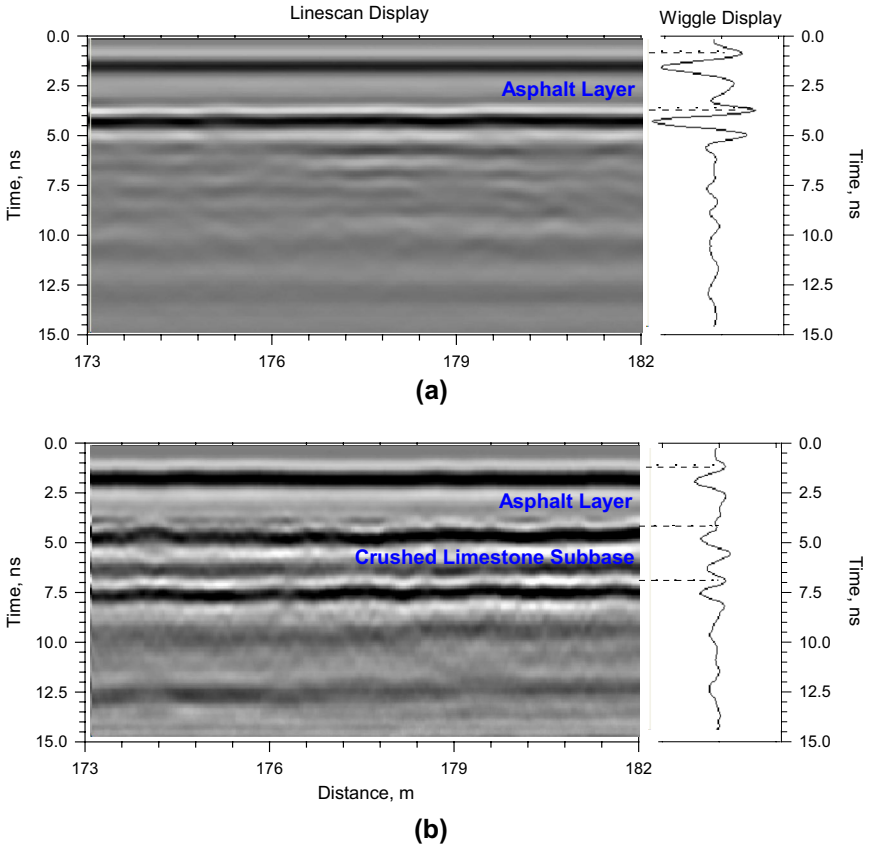

Figure 7. *In situ* GPR scans on 10th St. South section (a) on 03/12/14, (b) on 09/16/14.

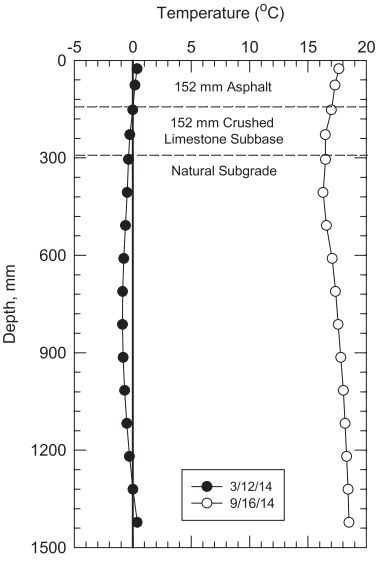

Figure 8. In situ ground temperatures during the two testing times.

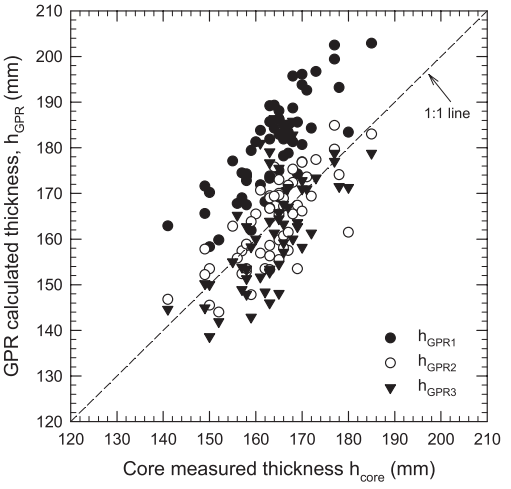

Figure 9. GPR estimated h_{GPR} vs. core measured asphalt layer thickness h_{core}.

clear transition between the two layers could not be identified in the GPR scans, and is therefore analysed as a single layer. This is attributed to the similar dielectric properties of the two materials as identified in the laboratory testing. The analysis herein is focused only on the CLS and RSB layers, as no transitions were identified in the layers beneath the RSB layers.

Thickness determination of foundation layers from GPR scans was not possible as the laboratory testing showed strong influence of moisture content on dielectric properties of the subbase layer material. The thickness of the base layers (h_{base}) determined from DCP tests (as illustrated in Figure 2) and the two-way travel times were used to determine ε_{GPR} of the subbase material. Volumetric moisture contents were determined using ε_{GPR} and Equation (3) for comparison between the test sections. The purpose of this analysis was to assess variations in the subbase layer moistures between the various test sections. The average ε_{GPR} and volumetric moisture content values determined from DCP test locations are shown in Figure 11.

Results indicated that on average, the volumetric moisture contents in the subbase layer varied from about 6% to 25%. The 8th St. test section showed the lowest values. Field permeability test results documented by White and Vennapusa [35] on 8th St. South section indicated that the CLS layer on this street yielded high saturated hydraulic conductivity and less non-uniformity (Average = 22.7 cm/s and coefficient of variation = 107%), compared to testing performed on 11th St. South section (Average = 1.8 cm/s and coefficient of variation = 172%) and 5th St. South section (Average = 13.2 cm/s and coefficient of variation = 207%). The 8th St. section consisted of more open-graded materials with less segregation and particle degradation compared to 11th St. and 5th St. sections.[35]

5. Key findings and conclusions

Following are key findings and conclusions from this study:

- The dielectric properties obtained from the independent dielectric measurement gauge used in this study correlated strongly with the values back-calculated from GPR and yielded $R^2 = 0.945$ with a standard error of 1.3 (Figure 4).

Table 4. Comparison between asphalt thicknesses measured from cores and predicted from GPR scans.

				h_{GPR1} (mm)		h_{GPR2} (mm)		h_{GPR3} (mm)	
Street	Asphalt layer description	No. of measurements	Average h_{core} (mm)	Average (mm)	Error (%)	Average (mm)	Error (%)	Average (mm)	Error (%)
1st / 2nd	50-mm HMAa surface with LAAc and 102-mm HMAa base with LAAc	16	163.3	178.8	10.3	163.2	3.6	156.3–175.6	3.9–8.5
3rd S. / 4th	50-mm WMAb surface with LAAc and 102-mm WMAb base with LAAc	10	165.5	183.5	11.3	165.5	2.7	160.9–175.6	2.7–5.1
7th / 8th	50-mm HMAa surface with HAAd and 102-mm HMAa base with LAAc	16	165.4	182.2	11.1	165.1	5.3	155.7–184.0	5.3–8.6
9th S. / 10th	50-mm WMAb surface with HAAd and 102-mm HMAa base with LAAc	11	160.1	173.9	9.5	159.8	3.8	151.0–169.9	4.8–7.2
11th	50-mm WMAb surface with HAAd and 102-mm WMAb base with LAAc	5	163.8	181.6	11.4	163.7	3.1	157.2–172.7	3.4–6.3

[a]Hot mix asphalt.
[b]Warm mix asphalt.
[c]Low absorbed aggregate.
[d]High absorbed aggregate.
[e]Error (%) = 100 × (root mean-squared error in reference to h_{core})/average h_{core}.

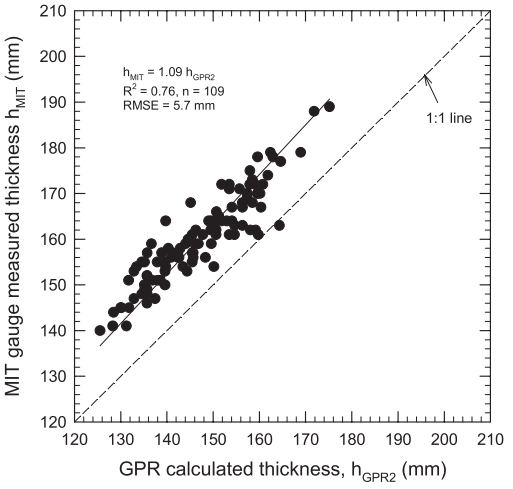

Figure 10. GPR vs. MIT gauge measured asphalt layer thickness.

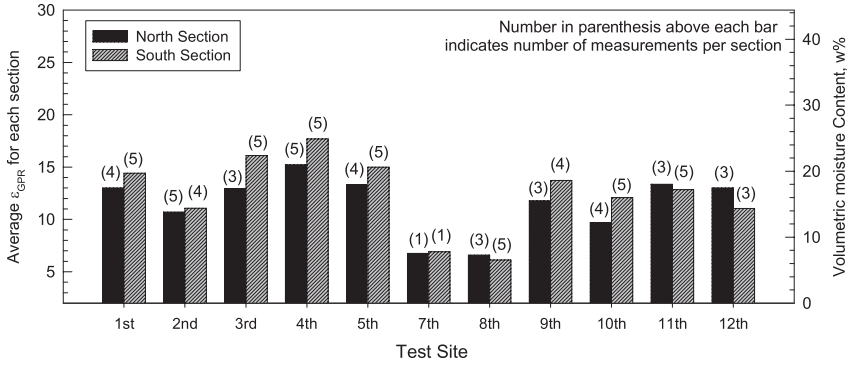

Figure 11. Estimated average *in situ* base layer E_{GPR} and volumetric moisture content for each street based on DCP measurements.

- A new database of dielectric properties of subgrade and base layer materials and chemically stabilised subgrade materials at different moisture contents is provided in this paper (Figures 5 and 6). Results indicated that the dielectric properties are sensitive to moisture content, as expected, and are sensitive to curing times for chemically stabilised soil due to the hydration process. PC- and FA-stabilised subgrade materials produced lower dielectric values than unstabilised subgrade materials.
- GPR surveys conducted during frozen condition did not properly differentiate variations in the foundation layers because of similar dielectric properties of those materials in a frozen condition (Figure 7). This was verified by conducting a simple laboratory box study with compacted pavement and foundation layers in frozen and unfrozen conditions (Figure 3).
- The estimated asphalt thicknesses (h_{GPR1}) using the ε_{GS3} values produced an average error of about 11% (Table 4). The estimated values (h_{GPR2} and h_{GPR3}) were close to the 1:1 line when compared with the measured values, when ε_{GPR} was used (see Figure 9).

The error values ranged between 2.7 and 8.6% h_{GPR3}, depending on the core sample selected in the analysis (Table 4). The average error reduced to 3.7% for h_{GPR3}, when average ε_{GPR} (based on multiple cores for each material type) was used in the analysis (Table 4). These errors are similar to those reported by others in the literature with air-coupled GPR antennas.

- Comparison between asphalt thickness measured using the MIT gauge and GPR (h_{GPR2}) indicated that the MIT gauge measurements were on average about 9% higher than estimated with GPR (Figure 10).
- GPR data were used to estimate volumetric moisture content of the granular subbase material. Results indicated that on average, the volumetric moisture contents in the subbase layer varied from about 6 to 25% (Figure 11). The variations are attributed to material segregation and degradation, and variations in aggregate gradations and permeability between the test sections.

List of Abbreviations and Notations

C Speed of light in air

CLS Crushed limestone

CMA Cold mix asphalt

CRM Complex refractive model

DCP Dynamic cone penetrometer

DOT Department of transportation

FA Fly ash

GPR Ground penetrating radar

GPS Global positioning system

GSSI Geophysical Survey Systems, Inc.

h_{core} Thickness of core

h_{GPR} Back-calculated thickness of asphalt from GPR measurements

h_{MIT} Thickness of asphalt measured using MIT gauge

HAA High absorption aggregate

HMA Hot mix asphalt

h_i Individual layer thickness

LAA low absorption aggregate

MIT Magnetic imaging tomography

N Porosity

PC Portland cement

PR Penetration resistance

RSB Reclaimed subbase

R^2 Coefficient of determination

SE Standard error of the estimate

t_i Time travel in each individual layer

w moisture content determined as fractional weight of water to total weight

WMA Warm mix asphalt

ε Dielectric constant or relative electrical permittivity

ε_b Base layer dielectric constant

ε_s Dry aggregate dielectric constant

ε_{GS3} Dielectric constant measured from GS3 device

ε_{GPR} Dielectric constant back-calculated from GPR measurements

θ_v Volumetric moisture content

Acknowledgements

Results presented in this paper were collected as part of a research project sponsored by the Iowa Department of Transportation (DOT) and Federal Highway Administration. Numerous officials from the Iowa DOT assisted in providing project access. All their help is greatly appreciated.

Disclosure statement

No potential conflict of interest was reported by the authors.

References

[1] AASHTO. Mechanistic-empirical pavement design guide: a manual of practice. Washington, DC: American Association of State Highway Officials and Transportation Officials; 2008.
[2] Al-Qadi IL, Lahouar S, Loulizi A. GPR: from the state-of-the-art to the state-of-the-practice. In: International Symposium of Non-destructive Testing in Civil Engineering. Proceedings BB85-CD; 2003 Sep.; Berlin, Germany: The German Society for Non-Destructive Testing (DGZfp). p. 16–19.
[3] AL-Qadi I, Lahouar S. Measuring layer thicknesses with GPR–theory to practice. Constr. Build. Mater. 2005;19:763–772.
[4] Al-Qadi IL, Leng Z, Lahouar S, et al. In-place hot-mix asphalt density estimation using ground-penetrating radar. Transp. Res. Rec.: J. Transp. Res. Board. 2010;2152:19–27.
[5] Lahouar S, Al-Qadi IL. Automatic detection of multiple pavement layers from GPR data. NDT & E Int. 2008;41:69–81.
[6] Cao Y, Guzina BB, Labuz JF. Pavement evaluation using ground penetrating radar. St. Paul (MN): Minnesota Department of Transportation; 2008.

[7] Evans R, Frost M, Stonecliffe-Jones M, et al. A review of pavement assessment using ground penetrating radar (GPR). In: Rogers CDF, Chignell RJ, editors. 12th International Conference on Ground Penetrating Radar. Proceedings; 2008 Jun. 16–19; Birmingham, UK; 2008.
[8] Plati C, Loizos A. Using ground-penetrating radar for assessing the structural needs of asphalt pavements. Nondestr. Test. Eval. 2012;27:273–284.
[9] Goel A, Das A. Nondestructive testing of asphalt pavements for structural condition evaluation: a state of the art. Nondestr. Test. Eval. 2008;23:121–140.
[10] Poikajärvi J, Peisa K, Herronen T, et al. GPR in road investigations – equipment tests and quality assurance of new asphalt pavement. Nondestr. Test. Eval. 2012;27:293–303.
[11] Moropoulou A, Avdelidis NP, Koui M, et al. Infrared thermography and ground penetrating radar for airport pavements assessment. Nondestr. Test. Eval. 2002;18:37–42.
[12] Loizos A, Plati C. Accuracy of pavement thicknesses estimation using different ground penetrating radar analysis approaches. NDT & E Int. 2007;40:147–157.
[13] Al-Qadi IL, Lahouar S, Loulizi A. Successful application of ground-penetrating radar for quality assurance-quality control of new pavements. Transp. Res. Rec.: J. Transp. Res. Board. 2003;1861:86–97.
[14] Grote K, Hubbard S, Harvey J, et al. Evaluation of infiltration in layered pavements using surface GPR reflection techniques. J. Appl. Geophys. 2005;57:129–153.
[15] White DJ, Becker P, Vennapusa PK, et al. Assessing soil stiffness of stabilized pavement foundations. Transp. Res. Rec.: J. Transp. Res. Board. 2013;2335:99–109.
[16] Daniels JJ. Fundamentals of ground penetrating radar. In: Symposium on the Application of Geophysics to Engineering and Environmental Problems. Proceedings; 1989 March 13–16; Environment and Engineering Geophysical Society; 1989.
[17] GSSI. GSSI handbook for RADAR inspection of concrete. Salem (NH): Geophysical Survey Systems, Inc; 2006.
[18] Loken MC. Use of ground penetrating radar to evaluate Minnesota roads. St. Paul (MN): Minnesota Department of Transportation; 2007.
[19] Davis JL, Annan AP. Ground-penetrating RADAR for high-resolution mapping of soil and rock stratigraphy. Geophys. Prospect. 1989;37:531–551.
[20] Willett DA, Rister B. Ground penetrating radar pavement layer thickness evaluation. Lexington: Kentucky Transportation Center; 2002.
[21] Irwin HL, Yang W, Stubstad R. Deflection reading accuracy and layer thickness accuracy of pavement layer moduli. Nondestructive testing of pavements and backcalculation of pavement layer moduli. West Conshohocken (PA): ASTM STP1026:229-44; 1989.
[22] Lalague A, Lebens MA, Hoff I. Accuracy of ground penetrating radar in pavement thickness evaluation – impact of interpretation errors. In: Transport Research Arena: Transport Solutions from Research to Deployment. Proceedings. 2014 Apr. 14–17; Paris, France: Institut Francais des Sciences et Technologies des Transports, de l'Aménagement et des Réseaux (IFSTTAR); 2014.
[23] Lalagüe A, Hoff I, Accuracy of ground penetrating radar in bituminous pavement thickness evaluation. In: Transport Research Arena 2010. Proceedings; 2014; Brussels, Belgium.
[24] Saarenketo T, Scullion T. Using electrical properties to classify the strength properties of base course aggregates. College Station (TX): Texas Transportation Institute; 1995.
[25] Halabe UB, Maser K, Kausel E. Condition assessment of reinforced concrete using EM waves. Cambridge (MA): Massachusetts Institute of Technology; 1989.
[26] Maser K, Scullion T. Influence of asphalt layering and surface treatments on asphalt base layer thickness computations using radar. Report No. TX-92-1923-1. College Station (TX): Texas Transportation Institute; 1992.
[27] Scullion T, Chen Y, Lau CL. COLORMAP-user's manual with case studies. Report No. FHWA/TX-96/1341-1. College Station (TX): Texas Transportation Institute; 1995.
[28] Topp GC, Davis JL, Annan AP. Electromagnetic determination of soil water content: measurements in coaxial transmission lines. Water Resour. Res. 1980;16:574–582.
[29] Grove J, Jones K, Ye D, et al. Nondestructive tests of thickness measurements for concrete pavements. Transp. Res. Rec.: J. Transp. Res. Board. 2012;2268:61–67.

[30] ASTM. ASTM D6951 – 03 standard test method for use of the dynamic cone penetrometer in shallow pavement applications. West Conshohocken (PA): ASTM International; 2003.
[31] Decagon. GS3 water content, EC and temperature sensors operator's manual. Pullman (WA): Decagon Devices, Inc.; 2015.
[32] ASTM. ASTM D698-13 Standard test methods for Laboratory Compaction Characteristics of Soil Using Standard Effort (12,400 ft-lbf/ft^3(600 kN-m/m^3)). West Conshohocken (PA): ASTM International; 2013.
[33] Hallikainen M. Dielectric properties of NaCl ice at 16 GHz. Report No. S-1107. Espoo, Finland: Helsinki University of Technology, Radio Laboratory; 1977.
[34] Makul N. Dielectric permittivity of various cement-based materials during the first 24 hours hydration. Open J. Inorg. Non-Met. Mater. 2013;3:53–57.
[35] White DJ, Vennapusa P. Rapid in situ measurement of hydraulic conductivity for granular pavement foundations. In: Abu-Farsakh M, Yu X, Hoyos LR, editors. Geo-Congress 2014 Technical Papers. Proceedings; 2014 Feb. 23–26; Atlanta (GA), USA: American Society of Civil Engineers; 2014. p. 3005–3014.